Research Article | Vol. 29, No. 10 / 10 May 2021 / Optics Express 14314

Optics EXPRESS

Milliradian precision ultrafast pulse control for spectral phase metrology

JACOB STAMM,[1] JORGE BENEL,[2] ESMERANDO ESCOTO,[3] GÜNTER STEINMEYER,[4,5] AND MARCOS DANTUS[1,6,*]

[1]Department of Chemistry, Michigan State University, East Lansing, MI 48824, USA
[2]Universidad Nacional de Ingeniería, Apartado, Lima, Peru 31139, USA
[3]Deutsches Elektronen-Synchrotron DESY, Notkestraße 85, 22607 Hamburg, Germany
[4]Max Born Institute for Nonlinear Optics and Short Pulse Spectroscopy, 12489 Berlin, Germany
[5]Department of Physics, Humboldt University, 12489 Berlin, Germany
[6]Department of Physics and Astronomy, Michigan State University, East Lansing, MI 48824, USA
[*]dantus@msu.edu

Abstract: A pulse-shaper-based method for spectral phase measurement and compression with milliradian precision is proposed and tested experimentally. Measurements of chirp and third-order dispersion are performed and compared to theoretical predictions. The single-digit milliradian accuracy is benchmarked by a group velocity dispersion measurement of fused silica.

1. Introduction

Ultrashort laser pulses have seen widespread use in scientific, medical, and industrial fields. The spectral phase within the bandwidth of the pulse determines their duration and performance, hence the need for external methods to measure and control. Multiple pulse characterization methods have been reviewed in the literature [1–5]. The accuracy with which the phase is measured and controlled impacts the reproducibility of experimental results, optimizes the peak intensity of the pulses, and allows one to use the pulses in metrological applications such as the generation of pulse trains [6,7]. The most studied methods have been Frequency-Resolved Optical Gating (FROG) [8] and Spectral Phase Interferometry for Direct Electric-Field Reconstruction (SPIDER) [9], with different optical implementations and retrieval algorithms. In terms of pulse shaper based methods, Multiphoton Intrapulse Interference Phase Scan (MIIPS), which scans a known phase such as chirp or a cosine function to measure the unknown spectral phase of the output pulses is one of the better known methods [10–21]. Here we propose and experimentally test a new approach that increases the precision of pulse-shaper-based characterization and compression to milliradian levels. The new method uses a pulse shaper to scan a sharp phase step to reveal very small residual amounts of spectral dispersion such as chirp and TOD. When this method is compared to benchmarks, the accuracy estimated by a group delay dispersion measurement of fused silica is within 0.02 fs^2, and the precision is estimated to be 1fs^2.

The use of a phase step to control non-linear optical signals has been explored by many groups following the pioneering work by Meshulach and Silberberg [22,23]. The combination of multiple π-phase steps, as in binary phase shaping, extends this concept to tailor multiple possible nonlinear optical transitions [24–26]. Extension of phase steps measurements to strong fields in atoms and molecules have also been reported [27–31] In some cases, optimum results have been observed for phase step values that are different than π, for example, in strong-fields ¾ π steps showed the largest influence on ion yield [30,31], and the enhancement of stimulated emission was found to be sensitive to the sign of ½ π phase steps [32]. Because the measurements shown here depend on differences observed when using steps of different signs, a π-step resulted in no difference.

#422739 https://doi.org/10.1364/OE.422739
Journal © 2021 Received 18 Feb 2021; revised 12 Apr 2021; accepted 13 Apr 2021; published 26 Apr 2021

Optics EXPRESS

The reported standard deviation achieved when measuring the spectral phase of ultrafast pulses has been discussed in the literature. Given that accurate measurement of the spectral phase is paramount to pulse characterization, benchmarking against materials with known group velocity dispersion (GVD) has become the norm [11,33–37]. In fact, pulse characterization methods are achieving accuracies that rival measurements obtained by spectral interferometry [38,39]. Applications in communications, quantum computing, and cryptography will require tight control of the spectral phase for low-noise output. As ultrafast lasers evolve, their metrology must evolve as well. Correction of the spectral phase to sub-radian accuracy is becoming a more important goal as ultrafast lasers see wider use in the various fields of science and industry. Here we present a method for measuring the spectral phase of ultrafast laser pulses with milliradian precision.

2. Theory

We focus on the measurement of small amounts of chirp and third-order dispersion (TOD) that cannot be measured or corrected by other means but can affect the reproducibility of experimental results or processes, for example, molecular fragmentation in strong fields [30,31]. Chirp and TOD are quantified here in the usual way, and their magnitude is given by β_2, and β_3 in the following expression

$$\varphi(\omega) = \frac{\beta_2}{2!}(\omega - \omega_0)^2 + \frac{\beta_3}{3!}(\omega - \omega_0)^3, \tag{1}$$

where ω_0 is the center frequency of the spectrum. Linear and constant terms are neglected as they give rise to the carrier-envelope phase and the group delay, which cannot be extracted in pulse characterization measurements. Higher-order dispersion will be treated in a subsequent publication. Moreover, for the first part of the theory, we assume the pulses to be Gaussian

$$\tilde{E}(\omega) \equiv \sqrt{S(\omega)}\exp\{-i\varphi(\omega)\} \tag{2}$$

where

$$S(\omega) = \exp\{-g^2(\omega - \omega_0)^2/\sigma_f^2\} \tag{3}$$

is the spectrum of the pulse, with a bandwidth σ_f full width at half maximum (FWHM), and $g = 2\sqrt{\ln 2}$. The pulse duration FWHM, τ_f, is related to its bandwidth by the time-bandwidth product (TBP) $\sigma_f\tau_f \geq g^2$, with equality when the pulse is transform-limited (TL). Note that the bandwidth is in angular frequency, dividing by 2π one gets the familiar factor 0.44127 used to determine if the TBP of a Gaussian pulse is near TL. The expression for the intensity of the TL pulse in the time domain is given by

$$I_{TL}(t) = \exp\{-g^2(t/\tau_f)^2\}. \tag{4}$$

The method proposed uses a $\pi/2$ phase step, which is a spectral phase that is 0 for the lower frequency section of the spectrum, and $\pi/2$ for the higher frequency section. Similarly, a $-\pi/2$ phase step is a spectral phase with 0 for the lower frequency section and $-\pi/2$ for the higher frequency section. The transition point between the 0 radian section and the $\pi/2$ radian section is called the step and may be shifted across the spectrum. A $+\pi/2$ spectral phase, along with the spectrum and the resulting second harmonic (SH), is shown in Fig. 1 in both frequency and wavelength scales to clarify the definitions used. The equation used for calculating the power spectrum of the second harmonic (SH) in terms of a spectral phase is given by [40,14]:

$$S(2\omega) = \left|\int_{-\infty}^{\infty}\sqrt{S(\omega+\Omega)}\sqrt{S(\omega-\Omega)}\exp[-i\{\varphi(\omega+\Omega)+\varphi(\omega-\Omega)\}]d\Omega\right|^2. \tag{5}$$

A contour plot which shows the SH spectra as a function of phase step position is shown in Figs. 2(a) and (b), for both positive and negative $\pi/2$ phase-step scans. Far from $\omega = \omega_0$, the step

Optics EXPRESS

has little or no influence on the SH spectrum. When the respective $\pm\pi/2$ steps are scanned over a TL pulse, no difference is observed in the SH spectra at all step positions. However, when the pulse has slight phase distortions such as chirp, high-order dispersion, or any other arbitrary nonlinear function, the positive and negative $\pi/2$ steps will yield different contours. This fact is the basis for the proposed measurement technique.

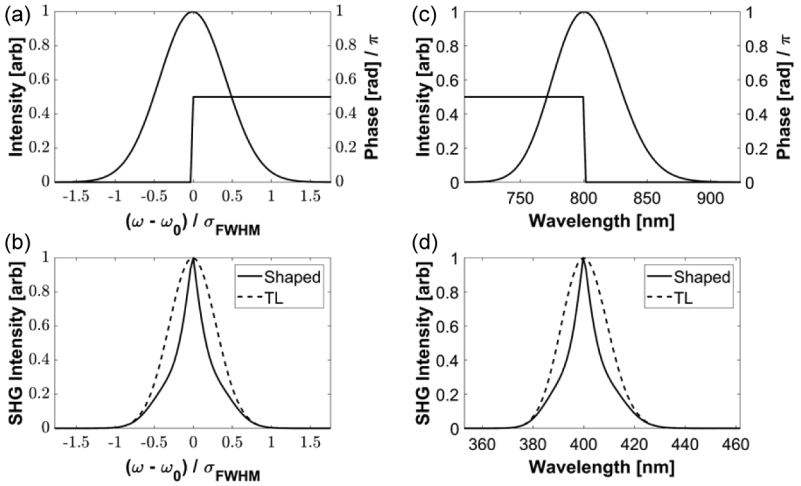

Fig. 1. The effect of a phase step on a femtosecond laser pulse. (a) Spectrum of a 15 fs pulse centered at ω_0 with a $+\pi/2$ phase step at the center frequency. (b) Second harmonic spectrum of the same pulse showing how the presence of the $+\pi/2$ phase step modifies the spectrum (bold line), compared to the second harmonic spectrum of a TL pulse without the phase step (dashed line). (c) Spectrum of a 15 fs pulse centered at 800 nm with a $+\pi/2$ phase step at the center frequency. (d) Second harmonic spectrum of the same pulse showing how the presence of the $+\pi/2$ phase step modifies the spectrum (bold line), compared to the second harmonic spectrum of a TL pulse without the phase step (dashed line).

The slight differences in the contour plots resulting from positive and negative $\pi/2$ step scans can be more easily visualized by taking the difference between the positive and negative contour plots. Chirp and TOD result in distinct features in the difference contour plot as shown in Figs. 2(c) and (d). Chirp leads to a difference contour with a trough (negative) and a peak (positive). The sign of the chirp dictates the order of the positive and negative peaks. Third order dispersion leads to a difference contour with four such features, with a node along the central frequency of the second harmonic spectrum. The amplitude of these features in the difference contour correlates with the amount of chirp or TOD, as described below.

The effect of chirp on a femtosecond laser pulse depends on its transform-limited FWHM, τ_{TL}, which is given by

$$\frac{\tau}{\tau_{TL}} = \sqrt{1 + \left(\frac{\beta_2 g^2}{\tau_{TL}^2}\right)^2}. \tag{6}$$

To obtain dimensionless expressions that are independent of pulse duration, as will be confirmed later, we define $\tilde{\beta}_2$ as the reduced chirp magnitude,

$$\tilde{\beta}_2 \equiv \beta_2 g^2 / \tau_{TL}^2 \tag{7}$$

which simplifies Eq. (6) to

$$\frac{\tau}{\tau_{TL}} = \sqrt{1 + \tilde{\beta}_2^2}. \tag{8}$$

Optics EXPRESS

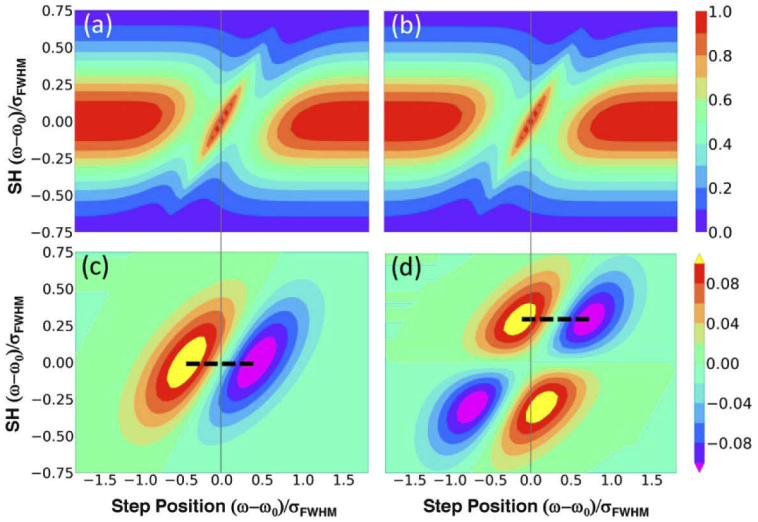

Fig. 2. Second harmonic intensity contour plots and difference contour plots resulting from scanning a π/2 phase step. (a) SHG intensity contour plot of a positive π/2 step scan. (b) SHG intensity contour plot of a negative π/2 step scan. (c) Difference between positive and negative contour plots when the 15-fs pulse has 10 fs^2 of residual chirp. (d) Difference between positive and negative contour plots when the 15-fs pulse has 300 fs^3 of residual TOD. The black dashed lines indicate places convenient for phase measurement.

From Fig. 1(b), we see that the SH spectrum is reduced by ½ at the position $0.3\sigma_f$, this reduction is symmetric with respect to the center of the spectrum for TL pulses. The presence of positive chirp causes an imbalance, where the attenuation is greater for higher frequencies. The imbalance becomes apparent when plotting the difference between scans obtained with positive and negative phase steps as shown in Fig. 2(c). The difference ΔS at the center of the SH spectrum as a function of the phase step position, δ, is given by

$$\Delta S(2\omega_0, \delta)_{difference} = \{S(2\omega_0, \delta)_+ - S(2\omega_0, -\delta)_-\}/S(2\omega_0, 0)_{TL}. \tag{9}$$

Normalization of the difference by the second harmonic maxima assuming the pulse is TL makes the method independent of pulse duration. The difference defined by Eq. (9) is plotted for $\tilde{\beta}_2 = 0.4$ in Fig. 3. We observe maximum and minimum values, as well as an inflection point where the difference changes sign, centered at $\delta = (\omega - \omega_0)/\sigma_f = 0$.

To quantify the residual chirp on the pulse, we find that the slope near $\delta = (\omega - \omega_0)/\sigma_f = 0$ provides a good measure of chirp. The slope varies sigmoidally as a function of reduced chirp $\tilde{\beta}_2$ according to

$$b_{slope}(\tilde{\beta}) = A \tanh(B\tilde{\beta}), \tag{10}$$

where A and B are parameters that define the sigmoidal dependence. When quantifying TOD from a contour plot such as that shown in Fig. 2(d), we find that $S(2\omega_0, -\sigma_f/2)_{difference} = 0$, which implies that chirp and TOD enter independently into this expression, and can be measured and corrected independently. In general, $S(2\omega_0, -\sigma_f/2)_{difference}$ has a maximum value for even order dispersion such as chirp and equals zero for odd order dispersoin as TOD. Quantification, therefore, seeks the slope of the line that joins the two top features at SH frequency $2(\omega - \omega_0) = 3\sigma/10$, see dashed black line in Fig. 2(d). The plot of that line as a function of phase step position looks very similar to that shown for chirp in Fig. 3, except that it is displaced from $\delta = (\omega - \omega_0)/\sigma_f = 0$ by $3\sigma/10$ for Gaussian pulses. The slope of that line, as a function of the phase step position, varies

Optics EXPRESS

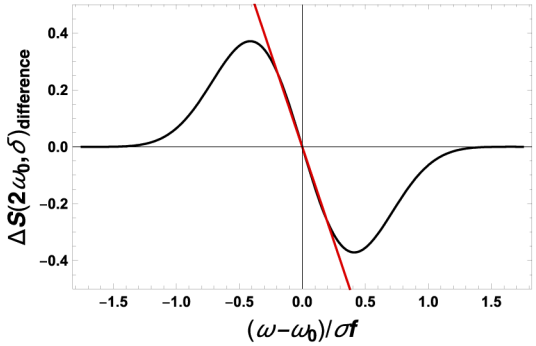

Fig. 3. Difference between the SH intensities obtained according to Eq. (9), for a 15 fs Gaussian pulse with chirp $\tilde{\beta}_2 = 0.4$ corresponding to 32.5 fs^2, as the phase step is scanned across the spectrum of the pulse (black). The slope at the center is indicated by a red line.

sigmoidally according to Eq. (10) as a function of the reduced TOD magnitude, defined as

$$\tilde{\beta}_3 \equiv \beta_3 g^3/\tau^3. \tag{11}$$

The SH generation process of a broadband pulse can essentially be modeled as sum-frequency process between individual Fourier components of the fundamental pulse, i.e., there is always a range of fundamental Fourier components that contribute to the SH signal at a fixed wavelength. And these components may either add constructively to the SH signal or act to reduce it. Switching a spectral portion by ±π/2 switches between these two cases. In general, we find that for even-order phase dispersion such as chirp Eq. (9) depends as −sin(α). Therefore, the

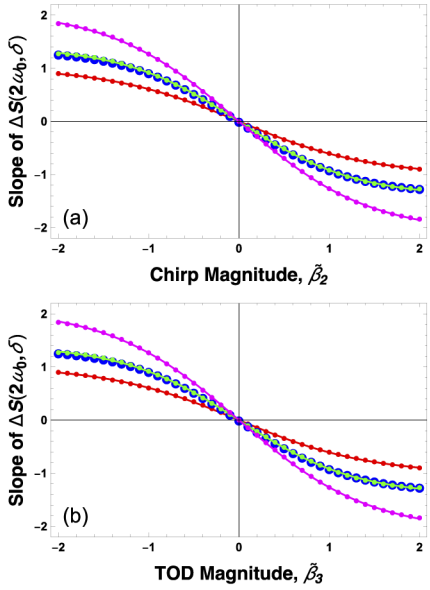

Fig. 4. Dependence of the slopes b_2 and b_3 as a function of reduced chirp (a) and TOD (b). The calculations were carried out for 15 fs Gaussian (blue), sech-squared (red), super-Gaussian (magenta), and skewed (green) spectral shapes. Detailed pulse parameters are given in Table 1. The dots correspond to values calculated from the general expression Eq. (9), while the lines are fits to the calculated points using Eq. (10).

Optics EXPRESS

sensitivity is maximized when α equals $(2n+1)\pi/2$, where n is an integer, as can be confirmed by Fig. 2(c) and Fig. 3. When the value of α is $n\pi$, the result for Eq. (9) is zero. For odd order phase dispersion, the value for Eq. (9) is zero as can be confirmed by the Fig. 2(d). This is why for measuring TOD we measure the features at SH frequency $2(\omega - \omega_0) = 3\sigma/10$.

We recognize that few ultrafast lasers produce Gaussian pulses, therefore, we extended the analysis to other common pulse spectral shapes, such as sech-squared, super-Gaussian, and a skewed spectral shape defined by the sum of two displaced Gaussian functions. The super-Gaussian function has an exponent greater than 2, thus causing the spectrum to be flat-topped. The respective function and parameters used are given in Table 1. In all cases we maintained the pulse duration fixed at 15 fs FWHM. Having defined the different spectra, we substituted them into Eq. (9), and found that they behaved like the pulses with a Gaussian spectrum, and that we could fit their dependence on chirp and TOD magnitude using Eq. (10), as shown in Figs. 4(a) and (b). For the analysis, the chirp and TOD magnitudes were calculated like those for 15 fs Gaussian pulses. The slope was calculated by fitting a line between ±0.2 of the respective bandwidth FWHM, and the TOD slope was calculated by finding the line where the variation is greatest, as shown in Fig. 1, for Gaussian pulses. The sigmoidal parameters depend on the spectral bandwidth of the different pulses [see Figs. 4(a) and (b)]. For example, the sech-squared spectrum has considerably larger wings than the super-Gaussian spectrum, which is flat-top and has very limited wings. Interestingly, the pulses with the skewed spectrum had essentially the same sigmoidal dependence on chirp and TOD. For experimental spectra that do not conform exactly to these mathematical models, it is important to create a calibration curve by using the shaper to introduce specific amounts of chirp and TOD. Without such calibration, the method will still detect spectral phase distortions, but the accuracy will be decreased.

Table 1. Spectral shape functions used to simulate the dependence of the slope given by Eq. (9) in the presence of chirp or TOD. In all cases, the pulse duration FWHM was fixed and is given as a function of the pulse duration except for super-Gaussian and skewed pulses where it is given as a number.

Gaussian	sech-squared	super-Gaussian	skewed
$S(\omega) = e^{-[\tau(\omega-\omega_0)/g]^2}$	$S(\omega) = \mathrm{sech}\left[\frac{\tau(\omega-\omega_0)\pi}{4\ln\left(1+\sqrt{2}\right)}\right]^2$	$S(\omega) = e^{-[\tau\lvert\omega-\omega_0\rvert/2.126]^3}$	$S(\omega) = 0.94e^{-[\tau(\omega-\omega_0+0.04)/1.26g]^2} + 0.33e^{-[\tau(\omega-\omega_0-0.08)/1.26g]^2}$
$\tau_f = 15$ fs	$\tau_f = 15$ fs	$\tau_f = 15$ fs	$\tau_f = 15$ fs
$\sigma_f = g^2/\tau_f$	$\sigma_f = \frac{\left[4\ln\left(1+\sqrt{2}\right)\right]^2}{2\pi\tau_f}$	$\sigma_f = 0.25$ fs^{-1}	$\sigma_f = 0.185$ fs^{-1}

3. Experimental results

Experiments are carried out using a titanium sapphire oscillator (Vitara, Coherent), operating at 80 MHz, capable of producing sub-20 fs pulses centered ~ 810 nm, shown in Fig. 5. The output of the laser is sent to a pulse shaper (MIIPS Box 640, Biophotonic Solutions Inc., IPG Photonics) and the output is then doubled in a 0.1 mm BBO (β-BaB_2O_4) crystal, as shown in Fig. 6. Pulse shaper calibration was essential for this work. We used the software included with the pulse shaper for confirming spectral alignment and calibration. The SH spectrum is collected with a compact spectrometer. For the measurements, we used multiphoton intrapulse interference phase scan (MIIPS) for pulse compression and obtained near TL pulses [11].

The experimental calibration parameters for chirp and TOD magnitude given the experimental spectrum of our pulses, which does not conform to a standard functional, was performed as follows. We scanned the π/2 step across the spectrum while recording the SH spectrum, we repeated the process for the negative π/2 step, and the difference between the two was written to a matrix and plotted as a contour map as shown in Fig. 2. This initial contour plot cannot be quantified yet, therefore it is treated as a background. We then use the pulse shaper to introduce

Optics EXPRESS

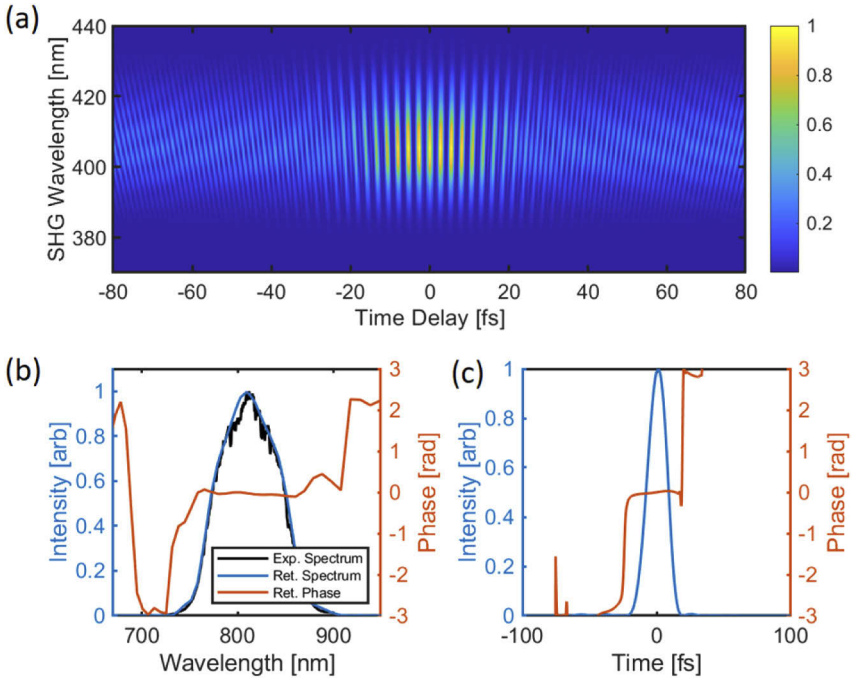

Fig. 5. Experimental characterization of the pulses. (a) Experimental 2D Interferometric FROG after compression using MIIPS and the method presented here. (b) Experimental and retrieved power spectrum of the laser with the retrieved spectral phase. (c) Retrieved temporal intensity and phase.

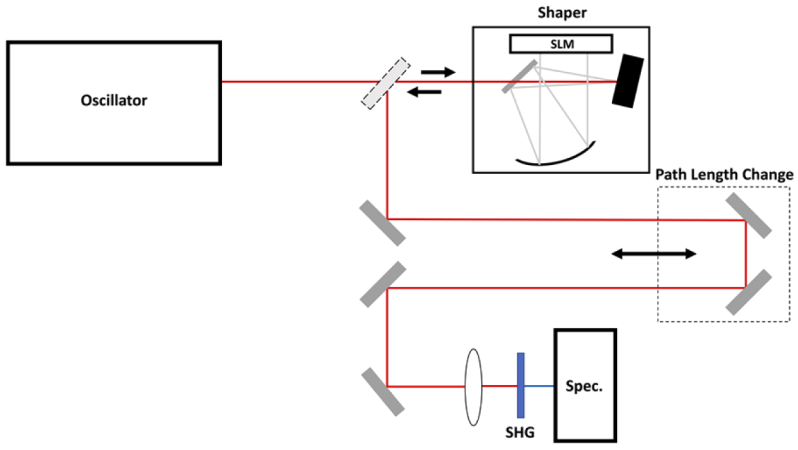

Fig. 6. Experimental setup with 4f pulse shaper.

Optics EXPRESS

a series of chirp values from which the contour maps defined by Eq. (9) can be analyzed after subtracting the background contour plot. From the difference values near $2\omega_0$ and step position $\delta = (\omega - \omega_0)/\sigma_f = \pm 2/10$, shown as a dashed line in Fig. 1(c), we obtain the slope for each chirp value. We then fit the slopes using Eq. (10) to obtain the sigmoidal function for chirp magnitude. The process is repeated to calibrate TOD measurements. The slope measurements are made at the position where a pair of features reaches their maximum and minimum values as shown in Fig. 1(d). Having obtained the calibration curves, one can perform spectral phase measurements without subtracting the background contour and the pulse shaper can be used to first eliminate chirp by entering a complementary chirp value to what is measured and then measuring and eliminating TOD to obtain TL pulses. The total phase distortion compensated corresponds to an accurate spectral phase measurement at the location of the SH crystal. Having eliminated SOD chirp and TOD, the pulses are now TL, with single-digit milliradian spectral phase deviation. We used the pulse shaper to obtain an experimental iFROG [41] measurement, shown in Fig. 5. Analysis of the iFROG measurement [34] revealed the pulse duration is 17 fs with < 1 fs^2 uncompensated chirp and ~ 20 fs^3 TOD.

The experimental calibration curves, shown in Fig. 7, were obtained for chirp and TOD values ranging from -1.5 to 1.5 for $\tilde{\beta}_2$ and -3 to 3 for$\tilde{\beta}_3$.

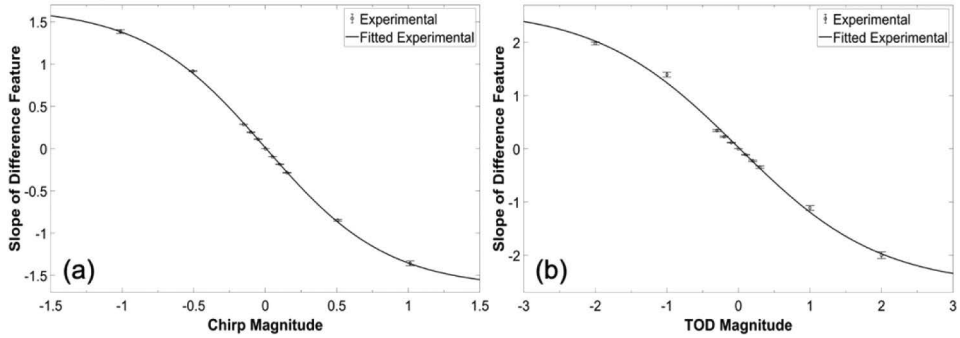

Fig. 7. Experimental values of the slopes b_2 (a) and b_3 (b) as a function of chirp and TOD, respectively. The dots correspond to measured values, while the line corresponds to Eq. (10) without experimental adjustment, respectively. Error bars are shown for $\pm 1\sigma$ error.

The data in Fig. 7 reproduces the theoretically predicted sigmoidal function. The sigmoidal function is parameterized into the form shown in Eq. (10). Experimental data may be fitted to this equation, although the parameters will differ from theoretical calculations due to a different spectral shape in the experimental setting. A comparison of the sigmoidal fit parameters obtained experimentally are compared with those obtained by simulation using the experimentally obtained spectrum and Eq. (9), is provided in Table 2. Once the experimental parameters have been acquired, the method can be used to measure small chirp or TOD values using the calibrated sigmoidal relationships as shown below.

Having confirmed the theory, we now seek to quantify the precision of the method. The first benchmark test is a measurement of the GVD of a 1-mm fused silica window. The laser's phase is corrected with MIIPS and this method, then the fused silica window is placed in the beam path. The $\pi/2$ steps are scanned, and the chirp is found as above from the difference contour. This method yields a GVD value of 36.18 ± 0.548 fs^2/mm, which agrees well with 36.162fs^2/mm using Sellmeier's formula and the optical constants for fused silica [42], and 36.2 ± 0.5 fs^2/mm MIIPS [11]. The value found with white-light interferometry 35.92 ± 0.05 fs^2/mm was less accurate [43].

This method is precise enough to measure very small chirp values such as the dispersion introduced by air. The group delay dispersion of air at 800 nm was measured under identical

Optics EXPRESS

Table 2. Simulation of the sigmoid parameters using the experimental spectrum and from experimental chirp and TOD data with 95% confidence interval.

	Theory (Experimental Spectrum)	Experimental
A (Chirp)	-3.181	-3.31 ± 0.10
B (Chirp)	1.230	1.31 ± 0.11
A (TOD)	-2.314	-2.61 ± 0.57
B (TOD)	0.403	0.51 ± 0.17

altitude and temperature conditions in our laboratory to be 20.05 ± 0.05 fs^2/m [36]. To test the method, we varied the path length of the laser pulses as they arrive at the SH crystal where they are frequency doubled. We measured the amount of chirp each time that the path length was increased by 0.254 m. We found that we could easily measure ~5.08 fs^2 additional dispersion.

The precision with which the spectral phase can be measured depends on the bandwidth of the pulses, and hence their TL pulse duration. For chirp, the dependence on pulse duration is quadratic and for TOD is cubic. The data shown here is pulse duration independent, because it is given in terms of $\tilde{\beta}_2$ and $\tilde{\beta}_3$, Eqs. (7) and (11). Here we translate the precision achieved to radians. Chirp and TOD spectral phase functions reach their maximum value at half of the FWHM. Therefore, we find that the maximum phase value reached at $\sigma_f/2$

$$\tilde{\varphi}(\sigma_f/2) = \frac{\beta_2}{2!}(\sigma_f/2)^2 = \frac{\tilde{\beta}_2\tau^2}{2!g^2}(g^2/2\tau)^2 = \tilde{\beta}_2 g^2/2!2^2, \tag{12}$$

for chirp and

$$\tilde{\varphi}(\sigma_f/2) = \frac{\beta_3}{3!}(\sigma_f/2)^3 = \frac{\tilde{\beta}_3\tau^3}{3!g^3}(g^2/2\tau)^3 = \tilde{\beta}_3 g^3/3!2^3, \tag{13}$$

for TOD. Therefore, having determined the precision with which we can measure $\tilde{\beta}_2$ and $\tilde{\beta}_3$ we can determine the accuracy of the method in terms of milliradians, and based on Eqs. (12) and (13). We performed an error analysis in our measurements and found our precision to be $\tilde{\beta}_2 = \pm 0.009$ and $\tilde{\beta}_3 = \pm 0.029$. Using Eqs. (12) and (13) we calculate the precision of this method to be 3.1 and 2.8 mrad, respectively. The result is independent of pulse duration. Based on these values we extrapolated to find minimum measurable chirp and TOD for pulse durations ranging

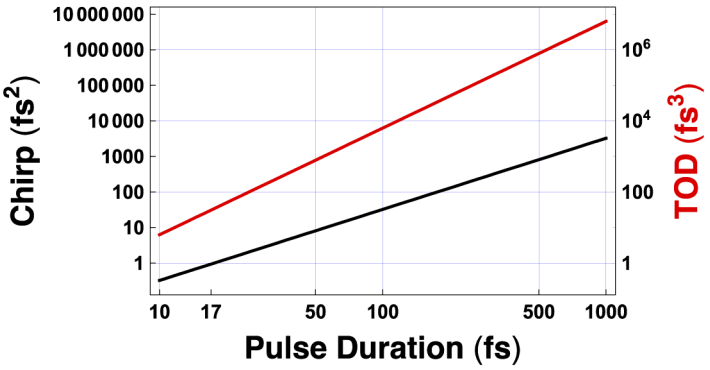

Fig. 8. Estimated chirp (black) and TOD (red) precision of the method based on the experimental measurements made with 17 fs pulses plotted as a log-log plot as a function of pulse duration.

Optics EXPRESS

from 10 fs to 1 ps, assuming the pulse shaper is configured for the bandwidth of the pulses. The results are plotted in Fig. 8. We see that for the 17 fs pulses used in our measurements we are sensitive to 1 fs^2 of chirp and 32 fs^3.

4. Conclusion

In summary, it has been predicted and demonstrated that single-digit milliradian phase variations on pre-compressed femtosecond pulses can be measured with the use of the $\pi/2$ scan method. The same method can be applied to pulses that have not been pre-compressed. Because the accuracy of the method decreases as the phase distortions increase, one or more iterations may be required before chirp and TOD are brought to a level where they can be accurately measured and compressed. We find that the measurement precision is limited primarily by laser stability and noise. This technique can be performed on top of commercially available pulse shaper based compression systems to reach levels of accuracy previously unreachable. This accuracy may find utility in areas of measurements of physical constants to metrology to the correction of experimental aberrations. Milliradian precision of the spectral phase is made easy with this method and can be streamlined into one system, reducing the labor needed to find the second and third order dispersion terms. This method allows for the generation of TL pulses with unprecedented accuracy, a fundamental need as the evolution of ultrafast lasers and their application in science and technology continues. The need to eliminate spectral phase distortions has recently been shown of interest in strong field laser-matter interactions [31], where minimal amounts of chirp can change the sign of enhancements observed via pulse shaping. Work is already underway in our lab to address arbitrary phase distortions that require higher order dispersion terms.

Funding. Office of Science (DE-SC0002325); Directorate for Mathematical and Physical Sciences (1836498).

Acknowledgments. We are grateful for the acquisition of some early data (not shown) by Dr. Shuai Li in the Dantus Group. Partial support for this work comes from the National Science Foundation Grant CHE1836498 for phase control of energy flow in molecules. J. Stamm is especially thankful for undergraduate research experience provided through that grant. J. Benel has been funded by OGI/VRI of the Universidad Nacional de Ingeniería, Peru. Additional support from the Chemical Sciences, Geosciences and Biosciences Division, Office of Basic Energy Sciences, Office of Science, U.S. Department of Energy Grant DE-SC0002325, experimental work aimed at understanding and controlling molecular dynamics in the gas phase.

Disclosures. MD: IPG Photonics Corp. (C), The authors declare no conflicts of interest.

References

1. I. A. Walmsley and C. Dorrer, "Characterization of ultrashort electromagnetic pulses," Adv. Opt. Photonics **1**(2), 308–437 (2009).
2. R. Trebino, P. Bowlan, P. Gabolde, X. Gu, S. Akturk, and M. Kimmel, "Simple devices for measuring complex ultrashort pulses," Laser Photonics Rev. **3**(3), 314–342 (2009).
3. D. R. Austin, T. Witting, and I. A. Walmsley, "High precision self-referenced phase retrieval of complex pulses with multiple-shearing spectral interferometry," J. Opt. Soc. Am. B **26**(9), 1818–1830 (2009).
4. M. Rhodes, G. Steinmeyer, and R. Trebino, "Standards for ultrashort-laser-pulse-measurement techniques and their consideration for self-referenced spectral interferometry," Appl. Opt. **53**(16), D1–D11 (2014).
5. C. Dorrer, "Spatiotemporal Metrology of Broadband Optical Pulses," IEEE J. Sel. Top. Quantum Electron. **25**(4), 1–16 (2019).
6. A. M. Weiner, *Ultrafast Optics* (Wiley, 2009).
7. M. Dantus, *Femtosecond Laser Shaping: From Laboratory to Industry* (CRC Press-Taylor & Francis Group, 2017).
8. R. Trebino, *Frequency-Resolved Optical Gating: The Measurement of Ultrashort Laser Pulses* (Springer Science & Business Media, 2000).
9. C. Iaconis and I. A. Walmsley, "Spectral phase interferometry for direct electric-field reconstruction of ultrashort optical pulses," Opt. Lett. **23**(10), 792–794 (1998).
10. V. V. Lozovoy, I. Pastirk, and M. Dantus, "Multiphoton intrapulse interference IV; Characterization and compensation of the spectral phase of ultrashort laser pulses," Opt. Lett. **29**(7), 775–777 (2004).

Optics EXPRESS

11. B. W. Xu, J. M. Gunn, J. M. Dela Cruz, V. V. Lozovoy, and M. Dantus, "Quantitative investigation of the multiphoton intrapulse interference phase scan method for simultaneous phase measurement and compensation of femtosecond laser pulses," J. Opt. Soc. Am. B **23**(4), 750–759 (2006).
12. I. Pastirk, X. Zhu, R. M. Martin, and M. Dantus, "Remote characterization and dispersion compensation of amplified shaped femtosecond pulses using MIIPS," Opt. Express **14**(19), 8885–8889 (2006).
13. I. Pastirk, B. Resan, A. Fry, J. MacKay, and M. Dantus, "No loss spectral phase correction and arbitrary phase shaping of regeneratively amplified femtosecond pulses using MIIPS," Opt. Express **14**(20), 9537–9543 (2006).
14. B. W. Xu, Y. Coello, V. V. Lozovoy, D. A. Harris, and M. Dantus, "Pulse shaping of octave spanning femtosecond laser pulses," Opt. Express **14**(22), 10939–10944 (2006).
15. D. A. Harris, J. C. Shane, V. V. Lozovoy, and M. Dantus, "Automated phase characterization and adaptive pulse compression using Multiphoton Intrapulse Interference Phase Scan in air," Opt. Express **15**(4), 1932–1938 (2007).
16. M. Dantus, V. V. Lozovoy, and I. Pastirk, "MIIPS characterizes and corrects femtosecond pulses," Laser Focus World **43**, 101–104 (2007).
17. Y. Coello, B. Xu, T. L. Miller, V. V. Lozovoy, and M. Dantus, "Group-velocity dispersion measurements of water, seawater, and ocular components using multiphoton intrapulse interference phase scan (MIIPS)," Appl. Opt. **46**(35), 8394–83401 (2007).
18. Y. Coello, V. V. Lozovoy, T. C. Gunaratne, B. Xu, I. Borukhovich, C.-H. Tseng, T. Weinacht, and M. Dantus, "Interference without an interferometer: a different approach to measuring, compressing, and shaping ultrashort laser pulses," J. Opt. Soc. Am. B **25**(6), A140–A150 (2008).
19. V. V. Lozovoy, B. Xu, Y. Coello, and M. Dantus, "Direct measurement of spectral phase for ultrashort laser pulses," Opt. Express **16**(2), 592–597 (2008).
20. D. Pestov, V. V. Lozovoy, and M. Dantus, "Single-beam shaper-based pulse characterization and compression using MIIPS sonogram," Opt. Lett. **35**(9), 1422–1424 (2010).
21. D. Pestov, A. Ryabtsev, G. Rasskazov, V. V. Lozovoy, and M. Dantus, "Single-beam single-shot measurement and correction of pulse phase and amplitude for ultrafast lasers," Opt. Eng. **53**(5), 051511 (2014).
22. D. Meshulach and Y. Silberberg, "Coherent quantum control of multiphoton transitions by shaped ultrashort optical pulses," Phys. Rev. A **60**(2), 1287–1292 (1999).
23. J. Degert, W. Wohleben, B. Shate, M. Motzkus, and B. Giranrd, "Realization of a Time-Domain Fresnel Lens with Coherent Control," Phys. Rev. Lett. **89**(20), 203003 (2002).
24. M. Comstock, V. V. Lozovoy, I. Pastirk, and M. Dantus, "Multiphoton intrapulse interference 6; binary phase shaping," Opt. Express **12**(6), 1061–1066 (2004).
25. V. V. Lozovoy and M. Dantus, "Systematic control of nonlinear optical processes using optimally shaped femtosecond pulses," ChemPhysChem **6**(10), 1970–2000 (2005).
26. V. V. Lozovoy, B. Xu, J. C. Shane, and M. Dantus, "Selective nonlinear optical excitation with pulses shaped by pseudorandom Galois fields," Phys. Rev. A **74**(4), 041805 (2006).
27. V. V. Lozovoy, X. Zhu, T. C. Gunaratne, D. A. Harris, J. C. Shane, and M. Dantus, "Control of molecular fragmentation using shaped femtosecond pulses," J. Phys. Chem. A **112**(17), 3789–3812 (2008).
28. M. Wollenhaupt, T. Bayer, N. V. Vitanov, and T. Baumert, "Three-state selective population of dressed states via generalized spectral phase-step modulation," Phys. Rev. A **81**(5), 053422 (2010).
29. B. D. Bruner, H. Suchowski, N. V. Vitanov, and Y. Silberberg, "Strong-field spatiotemporal ultrafast coherent control in three-level atoms," Phys. Rev. A **81**(6), 063410 (2010).
30. M. J. Michie, N. Ekanayake, N. P. Weingartz, J. Stamm, and M. Dantus, "Quantum coherent control of H_3^+ formation in strong fields," J. Chem. Phys. **150**(4), 044303 (2019).
31. S. Li, D. Sierra-Costa, M. J. Michie, I. Ben-Itzhak, and M. Dantus, "Control of electron recollision and molecular nonsequential double ionization," Commun. Phys. **3**(1), 35 (2020).
32. A. Konar, V. V. Lozovoy, and M. Dantus, "Stimulated Emission Enhancement Using Shaped Pulses," J. Phys. Chem. A **120**(12), 2002–2008 (2016).
33. L. Gallmann, D. Sutter, N. Matuschek, G. Steinmeyer, and U. Keller, "Techniques for the characterization of sub-10-fs optical pulses: a comparison," Appl. Phys. B **70**(S1), S67–S75 (2000).
34. J. Hyyti, E. Escoto, and G. Steinmeyer, "Pulse retrieval algorithm for interferometric frequency-resolved optical gating based on differential evolution," Rev. Sci. Instrum. **88**(10), 103102 (2017).
35. Y. Cai, Z. Chen, S. Zheng, H. Shangguan, X. Zeng, X. Lu, H. Wang, and S. Xu, "A compact, highly stable spectral shearing interferometer to accurately reconstruct ultrafast laser fields," Opt. Lasers Eng. **130**, 106081 (2020).
36. P. J. Wrzesinski, D. Pestov, V. V. Lozovoy, J. R. Gord, M. Dantus, and S. Roy, "Group-velocity-dispersion measurements of atmospheric and combustion-related gases using an ultrabroadband-laser source," Opt. Express **19**(6), 5163–5170 (2011).
37. P. Devi, V. V. Lozovoy, and M. Dantus, "Measurement of group velocity dispersion of solvents using 2-cycle femtosecond pulses: Experiment and theory," AIP Adv. **1**(3), 032166 (2011).
38. A. Börzsönyi, Z. Heiner, M. P. Kalashnikov, A. P. Kovács, and K. Osvay, "Dispersion measurement of inert gases and gas mixtures at 800 nm," Appl. Opt. **47**(27), 4856–4863 (2008).
39. S. Rivet, A. Bradu, F. Bairstow, H. Forrière, and A. Podoleanu, "Group refractive index and group velocity dispersion measurement by complex master slave interferometry," Opt. Express **26**(17), 21831–21842 (2018).

Optics EXPRESS

40. K. A. Walowicz, I. Pastirk, V. V. Lozovoy, and M. Dantus, "Multiphoton intrapulse interference 1; Control of multiphoton processes in condensed phases," J. Phys. Chem. A **106**(41), 9369–9373 (2002).
41. G. Stibenz and G. Steinmeyer, "Interferometric frequency-resolved optical gating," Opt. Express **13**(7), 2617–2626 (2005).
42. I. H. Malitson, "Interspecimen comparison of the refractive index of fused silica," J. Opt. Soc. Am. **55**(10), 1205–1209 (1965).
43. S. Diddams and J. C. Diels, "Dispersion measurements with white-light interferometry," J. Opt. Soc. Am. B **13**(6), 1120–1129 (1996).